

Cyclic three-level-pulse-area theorem for enantioselective state transfer of chiral molecules

Yu Guo,^{1,2,3} Xun Gong,² Songshan Ma,¹ and Chuan-Cun Shu^{1,*}

¹*Hunan Key Laboratory of Nanophotonics and Devices,*

School of Physics and Electronics, Central South University, Changsha 410083, China

²*Hunan Provincial Key Laboratory of Flexible Electronic Materials Genome Engineering,*

School of Physics and Electronic Science,

Changsha University of Science and Technology, Changsha 410114, China

³*The Key Laboratory of Low-Dimensional Quantum*

Structures and Quantum Control of Ministry of Education,

Hunan Normal University, Changsha 410081, China

Abstract

We derive a pulse-area theorem for a cyclic three-level system, an archetypal model for exploring enantioselective state transfer (ESST) in chiral molecules driven by three linearly polarized microwave pulses. By dividing the closed-loop excitation into two separate stages, we obtain both amplitude and phase conditions of three control fields to generate high fidelity of ESST. As a proof of principle, we apply this pulse-area theorem to the cyclohexylmethanol molecules ($C_7H_{14}O$), for which three rotational states are connected by the *a*-type, *b*-type, and *c*-type components of the transition dipole moments in both center-frequency resonant and detuned conditions. Our results show that two enantiomers with opposite handedness can be transferred to different target states by designing three microwave pulses that satisfy the amplitude and phase conditions at the transition frequencies. The corresponding control schemes are robust against the time delays between the two stages. We suggest that the two control fields used in the second stage should be applied simultaneously for practical applications. This work contributes an alternative pulse-area theorem to the field of quantum control, which has the potential to determine the chirality of enantiomers in a mixture.

* cc.shu@csu.edu.cn [he/him/his](https://orcid.org/0009-0001-9000-0000)

I. INTRODUCTION

Since Louis Pasteur first reported molecular chirality in 1848 [1], the theoretical and experimental study of chiral molecules has drawn increasing interest because of its fundamental importance in modern chemical and biochemical industries as well as quantum science [2–5]. Two enantiomers of chiral molecules with opposite handedness have the same components and configuration for spatial reflection. It implies that distinguishing enantiomers from each other, highly related to the discrimination, separation, and purification of chiral molecules, remains a formidable task by comparing general physical and chemical properties, such as boiling points, melting points, and densities. Based on chemical mechanisms and enantiomer-specific interactions with auxiliary substances, many spectroscopic techniques were established to detect enantiomers of chiral molecules with different handedness [6–8]. The traditional techniques, such as crystallization and chiral chromatography, are complicated and expensive and require significantly more protracted than seconds, leading to discrimination of chiral molecules out of reach.

By taking advantage of the sign difference property of optical rotations, it has become promising to select enantiomers by designing coherent quantum optical schemes [9–26]. The concept of the adiabatic passage techniques, such as stimulated Raman adiabatic passages [27, 28] and shortcuts to adiabaticity [29, 30], was proposed to generate efficient and robust detection and separation of chiral molecules [31–36]. In order to meet adiabatic criteria, the adiabatic passage techniques involve strict limitations on the control fields, and therefore, the corresponding control processes are usually slow and complicated. To that end, nonadiabatic schemes using much shorter durations of control pulses than the adiabatic approaches have been proposed to reach fast enantioselective excitation of chiral molecules [37, 38]. Experimentally, it has been demonstrated by using resonant microwave three-wave mixing (M3WM) techniques [39–46]. A common feature of both adiabatic and nonadiabatic control schemes usually involves a closed-loop quantum system by cyclic coupling of three molecular (i.e., rotational or rovibrational) states (as shown in Fig. 1), which are resonantly driven through the *a*-type, *b*-type, and *c*-type components of the transition dipole moments by a combination of three orthogonally polarized and phase-controlled microwave fields [47]. Since one of three cyclic couplings differs in the sign of the transition dipole moment in two opposite enantiomers, direct one-photon transition path from the ground state to a given target state constructively or destructively interferes with indirect two-photon transition path through an intermediate state, leading to enantioselective state transfer (ESST). Although the pulse areas

of the three control fields that can generate enantioselective excitation have been experimentally examined in M3WM experiments, there is still lacking a general pulse-areas theorem that can be used to directly calculate the amplitudes and phases of three time-dependent control pulses so as to gain insights into the underlying coherent quantum control mechanism.

In this paper, we focus on ESST and present a three-level pulse-areas theorem analysis. Previous works had derived the pulse area theorems for the three-level quantum systems with the ladder-, Λ - and V -type configurations [48–51], leading to many successful applications in coherent quantum control simulations and experiments [52–57]. Here, we take a strategy by dividing the closed-loop three-level excitation into two separated stages, i.e., combining a two-level excitation and a time-delayed-open-loop three-level transition. We obtain a pulse-areas theorem of the three-level system with a Δ -type configuration without applying the rotating-wave approximation. The derived pulse-areas theorem can calculate the exact amplitude and phase conditions for generating efficient ESST to the desired quantum state, which is examined in cyclohexylmethanol molecules ($C_7H_{14}O$) with different pulse sequences. This work provides an essential reference for coherent control of ESST using closed-loop three-level interaction schemes.

The remainder of this paper is organized as follows. In Sec. II, we describe the theoretical methods for obtaining a three-level pulse area theorem with cyclic coupling. We perform the numerical simulations to examine the derived pulse-areas theorem in Sec. III. Finally, we conclude with a summary in Sec. IV.

II. THEORETICAL METHOD AND NUMERICAL MODEL

A. Closed-loop three-level model

To describe our model, three rotational states of asymmetric top molecules, as shown in Fig. 1, are labeled as $|A\rangle$, $|B\rangle$ and $|C\rangle$ with a subscript L/R for the left/right-handed enantiomer. The energies E_A , E_B and E_C of three rotational states are identical for enantiomers. We mark three microwave control fields as $\vec{\mathcal{E}}_{a/b/c}(t)$, which drive the three states with the transition dipole moments $\vec{\mu}_a$, $\vec{\mu}_b$ and $\vec{\mu}_c$. As demonstrated in Refs. [47, 59], the ESST scheme with the use of linearly polarized control fields requires that a combination of control fields $\vec{\mathcal{E}}_a$, $\vec{\mathcal{E}}_b$ and $\vec{\mathcal{E}}_c$ with three orthogonal polarization directions along the directions of three dipole moment components $\vec{\mu}_a$, $\vec{\mu}_b$ and $\vec{\mu}_c$. To that end, we describe the time- and polarization-dependent electric fields of

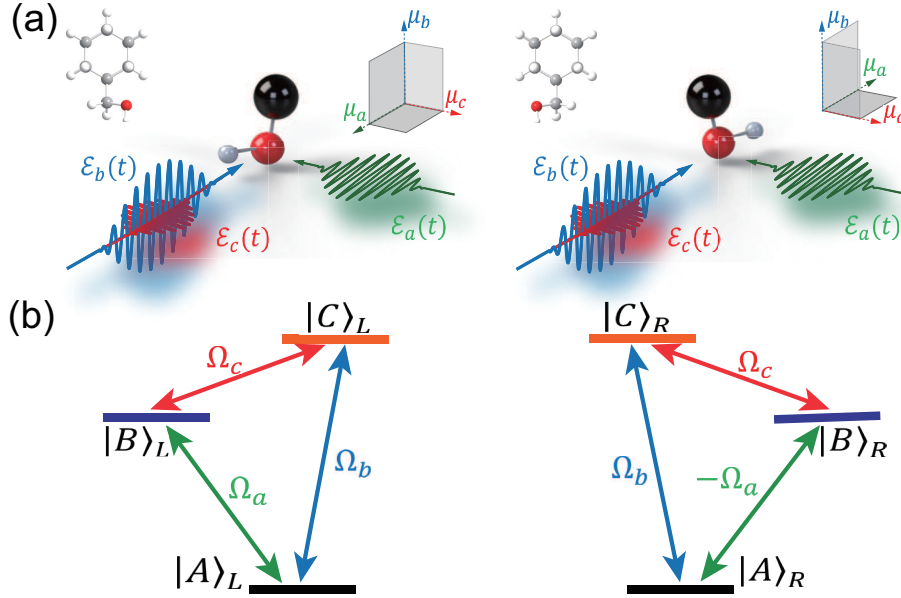


FIG. 1. Schematic illustration of enantioselective state transfer (ESST). (a) The space orientations of the transition dipole moments $\mu_{a/b/c}$ with respect to the polarization directions of three linearly polarized microwave pulses $\mathcal{E}_{a/b/c}(t)$. (b) The corresponding closed-loop transitions within three rotational states $|A\rangle$, $|B\rangle$ and $|C\rangle$. The transition frequencies and couplings between states are identical, except for a difference due to the sign difference in μ_a . The parameters of the cyclohexylmethanol molecules ($C_7H_{14}O$) are used for numerical simulations.

the three control fields by

$$\vec{\mathcal{E}}_{a/b/c}(t) = \vec{e}_{a/b/c} \mathcal{E}_{a/b/c} f_{a/b/c}(t) \cos[\omega_{a/b/c}(t - t_{a/b/c}) + \phi_{a/b/c}] \quad (1)$$

where $\vec{e}_{a/b/c}$, $\mathcal{E}_{a/b/c}$, $f_{a/b/c}(t)$, $\omega_{a/b/c}$, $t_{a/b/c}$, and $\phi_{a/b/c}$ denote the polarization direction, the strength, envelope function, center frequency, center time, and phase of $\vec{\mathcal{E}}_{a/b/c}(t)$, respectively. The triple product $\vec{\mu}_a \cdot (\vec{\mu}_b \times \vec{\mu}_c)$ is independent on the choice of the inertia principle axes a , b , and c , but is of opposite sign for the left- and right-handed enantiomers. For convenience, we specify that $\vec{\mu}_b$ and $\vec{\mu}_c$ are identical for two enantiomers, whereas $\vec{\mu}_a$ changes sign with the handedness. Thus, the Hamiltonian of two different handed-enantiomers in the presence of the control fields can be written as

$$H^{L,R}(t) = \begin{pmatrix} E_A & \pm\Omega_a(t) & \Omega_b(t) \\ \pm\Omega_a(t) & E_B & \Omega_c(t) \\ \Omega_b(t) & \Omega_c(t) & E_C \end{pmatrix}, \quad (2)$$

where the three cyclic couplings read $\Omega_a(t) = -\mu_a \mathcal{E}_a(t)$, $\Omega_b(t) = -\mu_b \mathcal{E}_b(t)$ and $\Omega_c(t) = -\mu_c \mathcal{E}_c(t)$.

We now analyze how to achieve enantioselective excitation of a given target state from a given initial state. We assume that two enantiomers are initially in the state $|A\rangle$, and the control target can be either the excited state $|B\rangle$ or $|C\rangle$. For the choice of $|C\rangle$ as the target, there are a direct one-photon transition $|A\rangle \leftrightarrow |C\rangle$ and an indirect two-photon transition $|A\rangle \leftrightarrow |B\rangle \leftrightarrow |C\rangle$, which form the closed-loop interaction scheme. If we take $|B\rangle$ as the target, two transition paths correspond to a direct one $|A\rangle \leftrightarrow |B\rangle$ and an indirect one $|A\rangle \leftrightarrow |C\rangle \leftrightarrow |B\rangle$. Since it remains difficult to derive an analytical solution by directly using the Hamiltonian in Eq. (2), we use a strategy by dividing the excitation processes into two stages.

B. Control conditions for ESST to $|C\rangle$

1. Analytical solution for a two-level system

For the ESST to $|C\rangle$, we assume that the coupling Ω_a is turned on at the initial time t_0 and off it at a time t_1 before the couplings Ω_b and Ω_c . Thus, the system is reduced into a two-level system, and the corresponding Hamiltonian reads

$$H_1^{L,R}(t) = \begin{pmatrix} E_A & \pm\Omega_a(t) \\ \pm\Omega_a(t) & E_B \end{pmatrix}. \quad (3)$$

Without using the rotating wave approximation, the evolution of the system in the interaction picture can be described by using the unitary operator

$$U_1^{L,R}(t, t_0) = U_1^{L,R}(t_0, t_0) - i \int_{t_0}^t dt' H_{1I}^{L,R}(t') U_1^{L,R}(t', t_0) \quad (4)$$

where $H_{1I}^{L,R}(t) = \exp(iH_{10}t) [\pm\Omega_a(t) (|A\rangle\langle B| + |B\rangle\langle A|)] \exp(-iH_{10}t)$ with the field-free Hamiltonian of the two-level system $H_{10} = E_A |A\rangle\langle A| + E_B |B\rangle\langle B|$. By involving the first-order the Magnus expansion [58], the time-dependent unitary operator $U_1^{L,R}(t, t_0)$ can be given by [50, 51, 54, 55]

$$U_1^{L,R}(t, t_0) = \cos |\theta_a(t)| (|A\rangle\langle A| + |B\rangle\langle B|) \\ \mp i \sin |\theta_a(t)| \left[\frac{|\theta_a(t)|}{\theta_a^*(t)} |B\rangle\langle A| + \frac{|\theta_a(t)|}{\theta_a(t)} |A\rangle\langle B| \right] \quad (5)$$

in terms of the complex pulse area $\theta_a(t) = \int_{t_0}^t \Omega_a(t') \exp(i\omega_{AB}t') dt'$ with $\omega_{AB} = E_B - E_A$. By considering the left and right-handed enantiomers initially in the ground state $|A\rangle$, an analytic

solution for the wave-function of the two-level system can be obtained by

$$\begin{aligned} |\psi_1^{L,R}(t)\rangle &= U_1^{L,R}(t, t_0) |A\rangle \\ &= \cos |\theta_a(t)| |A\rangle \mp i \frac{|\theta_a(t)|}{\theta_a^*(t)} \sin |\theta_a(t)| |B\rangle. \end{aligned} \quad (6)$$

2. Analytical solution for a three-level system

After the coupling Ω_a off at t_1 , we turn on the couplings Ω_b and Ω_c . The Hamiltonian in Eq. (2) is reduced into

$$H_2^{L,R}(t) = \begin{pmatrix} E_A & 0 & \Omega_b(t) \\ 0 & E_B & \Omega_c(t) \\ \Omega_b(t) & \Omega_c(t) & E_C \end{pmatrix}. \quad (7)$$

The corresponding time-dependent unitary operator can be given by

$$U_2^{L,R}(t, t_1) = U_2^{L,R}(t_1, t_1) - i \int_{t_1}^t dt' H_{2I}^{L,R}(t') U_2^{L,R}(t', t_1) \quad (8)$$

where $H_{2I}^{L,R}(t) = \exp(iH_{20}t) [\Omega_b(t)(|A\rangle\langle C| + |C\rangle\langle C|) + \Omega_c(t)(|C\rangle\langle B| + |B\rangle\langle C|)] \exp(-iH_{20}t)$ with the field-free Hamiltonian of the three-level system $H_{20} = E_A|A\rangle\langle A| + E_B|B\rangle\langle B| + E_C|C\rangle\langle C|$. By making the first-order Magnus expansion of the unitary operator $U_2^{L,R}(t, t_1)$, the time-dependent wave function of two enantiomers can be given by

$$\begin{aligned} |\psi_2^{L,R}(t)\rangle &= U_2^{L,R}(t, t_1) |\psi_1^{L,R}(t_1)\rangle \\ &= \left[\cos |\theta_a(t_1)| \frac{|\theta_c(t)|^2 + |\theta_b(t)|^2 \cos \theta(t)}{\theta^2(t)} \mp i \sin |\theta_a(t_1)| \zeta(t) \frac{|\theta_a(t_1)|}{\theta_a^*(t_1)} \right] |A\rangle \\ &\quad + \left[\cos |\theta_a(t_1)| \zeta^*(t) \mp i \sin |\theta_a(t_1)| \frac{|\theta_a(t_1)|}{\theta_a^*(t_1)} \frac{|\theta_b(t)|^2 + |\theta_c(t)|^2 \cos \theta(t)}{\theta^2(t)} \right] |B\rangle \\ &\quad - \frac{\sin \theta(t)}{\theta(t)} \left[i \cos |\theta_a(t_1)| \theta_b(t) \pm \sin |\theta_a(t_1)| \theta_c(t) \frac{|\theta_a(t_1)|}{\theta_a^*(t_1)} \right] |C\rangle, \end{aligned} \quad (9)$$

where $\zeta(t) = \theta_c(t) \theta_b^*(t) [\cos \theta(t) - 1] / \theta^2(t)$ and $\theta(t) = \sqrt{|\theta_b(t)|^2 + |\theta_c(t)|^2}$ in terms of the complex pulse areas $\theta_b(t) = \int_{t_1}^t \Omega_b(t') \exp(i\omega_{AC}t') dt'$ and $\theta_c(t) = \int_{t_1}^t \Omega_c(t') \exp(i\omega_{BC}t') dt'$ with the transition frequencies $\omega_{BC} = E_C - E_B$ and $\omega_{AC} = E_C - E_A$.

To entirely transfer the left-handed enantiomer to the state $|C\rangle$ while keeping the right-handed one unpopulated at the final time t_f , the complex pulse areas should satisfy the following two

relations

$$\left| \frac{\sin \theta(t_f)}{\theta(t_f)} \left[i\theta_b(t_f) \cos |\theta_a(t_1)| + \frac{|\theta_a(t_1)| \theta_c(t_f)}{\theta_a^*(t_1)} \sin |\theta_a(t_1)| \right] \right| = 1, \quad (10)$$

$$\left| \frac{\sin \theta(t_f)}{\theta(t_f)} \left[i\theta_b(t_f) \cos |\theta_a(t_1)| - \frac{|\theta_a(t_1)| \theta_c(t_f)}{\theta_a^*(t_1)} \sin |\theta_a(t_1)| \right] \right| = 0, \quad (11)$$

From the Eq. (11), we can derive

$$\frac{\theta_c(t_f)}{\theta_a^*(t_1)} = \frac{i\theta_b(t_f) \cos |\theta_a(t_1)|}{|\theta_a(t_1)| \sin |\theta_a(t_1)|}. \quad (12)$$

By inserting Eq. (12) into Eq. (10), we can obtain a relation

$$4 \left| \theta_b(t_f) \right|^2 \sin^2 \theta(t_f) \cos^2 |\theta_a(t_1)| = \theta^2(t_f). \quad (13)$$

This relation can be fulfilled when the three control fields satisfy the amplitude conditions

$$\begin{aligned} \left| \theta_b(t_f) \right| &= \left| \theta_c(t_f) \right| = \frac{1}{\sqrt{2}} \left(k + \frac{1}{2} \right) \pi, (k \in N) \\ \left| \theta_a(t_1) \right| &= \left(k' + \frac{1}{4} \right) \pi, (k' \in N). \end{aligned} \quad (14)$$

Furthermore, we insert Eq. (14) into Eq. (12) with $\theta_b = -|\theta_b| \exp(-i\phi_b)$, $\theta_c = -|\theta_c| \exp(-i\phi_c)$ and $\theta_a = -|\theta_a| \exp(-i\phi_a)$. We find that the three control fields satisfy the following phase condition,

$$\phi_a + \phi_c - \phi_b = \left(2l + \frac{1}{2} \right) \pi, (l \in Z). \quad (15)$$

Similarly, we can use the same amplitude conditions as that in Eq. (14) to achieve complete ESST to $|C\rangle$ of the right-handed enantiomer by using the phase condition of $\phi_a + \phi_b - \phi_c = (2l - 1/2)\pi, (l \in Z)$. It implies that a π flip of the phase on one of three control fields can result in opposite ESST. To that end, the handedness of enantiomers can be determined by measuring the population in the state $|C\rangle$.

C. Control conditions for ESST to $|B\rangle$

For ESST to $|B\rangle$, we apply the coupling Ω_b before the couplings Ω_a and Ω_c , which results in a coherent superposition state of $|A\rangle$ and $|C\rangle$. As demonstrated above by involving the first-order Magnus expansion and further mathematical derivations, an analytic wave-function of the

three-level Λ -type system can be given by

$$\begin{aligned}
|\psi_2^{L,R}(t)\rangle = & \left[\cos |\theta_b(t_1)| \frac{|\theta_c(t)|^2 + |\theta_a(t)|^2 \cos \theta(t)}{\theta^2} \mp i \sin |\theta_b(t_1)| \xi^*(t) \frac{|\theta_b(t_1)|}{\theta_b^*(t_1)} \right] |A\rangle \\
& - \frac{\sin \theta(t)}{\theta(t)} \left[\sin |\theta_b(t_1)| \theta_c^*(t) \frac{|\theta_b(t_1)|}{\theta_b^*(t_1)} \pm i \cos |\theta_b(t_1)| \theta_a(t) \right] |B\rangle \\
& - \left[i \sin |\theta_b(t_1)| \frac{|\theta_b(t_1)| |\theta_a(t)|^2 + |\theta_c(t)|^2 \cos \theta(t)}{\theta_b^*(t_1) \theta^2(t)} \mp \cos (|\theta_b(t_1)|) \xi(t) \right] |C\rangle, \quad (16)
\end{aligned}$$

where $\xi(t) = \theta_c(t) \theta_a(t) [\cos \theta(t) - 1] / \theta^2(t)$ and $\theta(t) = \sqrt{|\theta_a(t)|^2 + |\theta_c(t)|^2}$.

To entirely transfer the left-handed enantiomer to the state $|B\rangle$ at the final time t_f , but the right-handed one is not populating, we have

$$\left| \frac{\sin \theta(t_f)}{\theta(t_f)} \left[\sin |\theta_b(t_1)| \theta_c^*(t_f) \frac{|\theta_b(t_1)|}{\theta_b^*(t_1)} + i \cos |\theta_b(t_1)| \theta_a(t_f) \right] \right| = 1, \quad (17)$$

$$\left| \frac{\sin \theta(t_f)}{\theta(t_f)} \left[\sin |\theta_b(t_1)| \theta_c^*(t_f) \frac{|\theta_b(t_1)|}{\theta_b^*(t_1)} - i \cos |\theta_b(t_1)| \theta_a(t_f) \right] \right| = 0. \quad (18)$$

Furthermore, we can obtain the amplitude condition for the three control fields

$$\begin{aligned}
|\theta_a(t_f)| &= |\theta_c(t_f)| = \frac{1}{\sqrt{2}} \left(k + \frac{1}{2} \right) \pi, (k \in N) \\
|\theta_b(t_1)| &= \left(k' + \frac{1}{4} \right) \pi, (k' \in N). \quad (19)
\end{aligned}$$

The ESST to $|B\rangle$ of the left-handed enantiomer can be reached by using the phase condition

$$\phi_a + \phi_c - \phi_b = \left(2l - \frac{1}{2} \right) \pi, (l \in Z). \quad (20)$$

The amplitude conditions by Eq. (19) in forms are the same as Eq. (13) with different orders. That is, the orders of the three pulses are interchangeable, dependent on the choice of the target state. From the phase condition in Eq. (20), we can find that a π flip of the phase on one of three control fields can also lead to opposite ESST. Since our schemes that divide the closed-loop excitation schemes into two stages are different from previous works [18–20, 36, 44], which turned on the direct one-photon transition path before the two-photon one, these amplitude and phase conditions provide an alternative way to achieve ESST within a cyclic three-level systems in chiral molecules.

Note that the amplitude conditions of $|\theta_{a/b}(t_f)| = \pi/4$ and $|\theta(t_f)| = \sqrt{|\theta_{b/a}(t_f)|^2 + |\theta_c(t_f)|^2} = \pi/2$ are equivalent to that with the use of $\pi/2$ and π pulses, for which a scale of $1/2$ factor comes from the definition of the complex pulse-areas without using the rotating wave approximation and the

resonant excitation conditions. To show the advantage of using the complex pulse-areas, we can have a frequency-domain analysis for the control fields

$$\mathcal{E}_{a/b/c} = \frac{1}{\pi} \int_{t_0}^{t_f} d\omega \mathcal{A}_{a/b/c}(\omega) e^{i\phi_{a/b/c}(\omega)} e^{i\omega t} \quad (21)$$

where $\mathcal{A}_{a/b/c}(\omega)$ and $\phi_{a/b/c}(\omega)$ are the spectral amplitude and phase, respectively. We can find that the values of $\theta_{a/b/c}(t_f)$ depend only on $\mathcal{A}_{a/b/c}(\omega)$ and $\phi_{a/b/c}(\omega)$ of three control fields at transition frequencies ω_{AB} , ω_{AC} and ω_{BC} . Thus, our definitions of the complex pulse areas can also be applied to the pulsed control fields whose center frequencies are detuned away from the transition frequencies. In Sec. III, we present simulations to examine the amplitude and phase conditions for both center-frequency resonant and detuned microwave excitation schemes.

III. RESULTS AND DISCUSSION

We perform the numerical simulations in the cyclohexylmethanol molecules. Three rotational states of $|1_{01}\rangle$, $|2_{02}\rangle$, and $|2_{12}\rangle$ are used as $|A\rangle$, $|B\rangle$, and $|C\rangle$. The transition frequencies between states are $\omega_{AB} = 4720\text{MHz}$, $\omega_{BC} = 2339\text{MHz}$, and $\omega_{AC} = 7059\text{MHz}$, and the transition dipole moments take the values of $\mu_a = 0.4\text{Debye}$, $\mu_b = 1.2\text{Debye}$ and $\mu_c = 0.8\text{Debye}$ [18, 46]. In our simulations, we take three control fields with the Gaussian profile as follows

$$\mathcal{E}_{a/b/c}(t) = \sqrt{\frac{2}{\pi}} \frac{A_{a/b/c}}{\tau_0} \exp\left[-\frac{(t - t_{a/b/c})^2}{2\tau_0^2}\right] \cos\left[\omega_{q/p/s}(t - t_{a/b/c}) + \phi_{a/b/c}\right]. \quad (22)$$

This description of the control fields is convenient for determining the field strengths $\mathcal{E}_{a/b/c}$ for any accessible duration τ_0 . By choosing constant values of $A_{a/b/c}$, we can see that the complex pulse-areas $\theta_{a/b/c}(t_f)$ with such descriptions do not depend on the duration τ_0 . Thus, this scheme avoids the strict limitations by the adiabatic criterion, providing a way to design fast control schemes using much shorter pulse duration than the adiabatic scenario. For practical applications, however, we need to balance the choice of pulse duration τ_0 , so that unwanted transitions to neighboring energy levels could be avoided by using narrowband pulses.

For the cyclohexylmethanol molecules, there exists a rotational state $|1_{11}\rangle$ with the energy slightly below the state $|B\rangle$, referred as the state $|B'\rangle$, which can be connected to the excited state $|C\rangle$ via the a -type transition in $\omega_{B'C} = 4484\text{MHz}$ and to the ground state $|A\rangle$ via the c -type transition in $\omega_{AB'} = 2575\text{MHz}$. To this end, we include this state with a four-level model to perform the

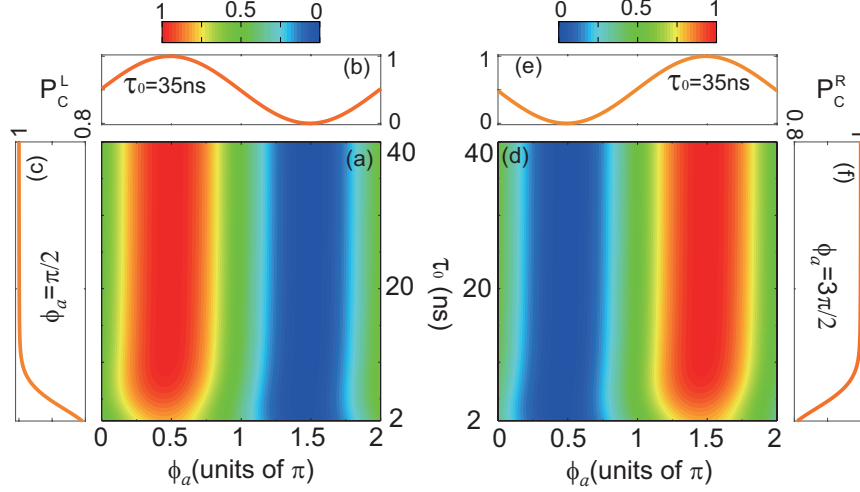


FIG. 2. Chiral dependence of ESST on the phase for the target state $|C\rangle$. (a) The final population of the left-handed enantiomer $P_C^L(t_f)$ versus the duration τ_0 and phase ϕ_a in a range of $[0, 2\pi]$, and the corresponding cut lines at (b) $\tau_0 = 35\text{ns}$ and (c) $\phi_a = \pi/2$. (d)-(f) The same plots as (a)-(c) for the right-handed enantiomer except for $\phi_a = 3\pi/2$ in (f).

numerical simulations. The corresponding field-molecule interaction Hamiltonian reads.

$$H_c^{L,R}(t) = \begin{pmatrix} 0 & \Omega'_c(t) & \pm\Omega_a(t) & \Omega_b(t) \\ \Omega'_c(t) & 0 & 0 & \pm\Omega'_a(t) \\ \pm\Omega_a(t) & 0 & 0 & \Omega_c(t) \\ \Omega_b(t) & \pm\Omega'_a(t) & \Omega_c(t) & 0 \end{pmatrix}, \quad (23)$$

where we take the additional couplings $\Omega'_a(t) = -\mu'_a \mathcal{E}_a(t)$ and $\Omega'_c(t) = -\mu'_c \mathcal{E}_c(t)$ with $\mu'_a = \mu_a$ and $\mu'_c = \mu_c$ in our simulations. The time-dependent unitary operator in the interaction picture can be numerically computed by

$$U^{L,R}(t, t_0) = U^{L,R}(t_0, t_0) - i \int_{t_0}^t dt' H_I^{L,R}(t') U^{L,R}(t', t_0), \quad (24)$$

where $U^{L,R}(t_0, t_0) = \mathbb{I}$ and $H_I^{L,R}(t) = \exp(iH_0 t) [H_c^{L,R}(t)] \exp(-iH_0 t)$ with the field-free Hamiltonian $H_0 = \sum_{X=A}^C E_X |X\rangle\langle X|$. By projecting the unitary operator $U^{L,R}(t, t_0)$ onto the initial state $|A\rangle$, we can obtain the time-dependent wave function of the system $|\psi^{L,R}(t)\rangle = U^{L,R}(t, t_0)|A\rangle$ without using the first-order Magnus expansion. Thus, the time-dependent population in the state $|X\rangle$ can be calculated by $P_X^{L/R}(t) = |\langle X|\psi^{L,R}(t)\rangle|^2$ with $X = A, B', B, C$.

A. ESST to $|C\rangle$

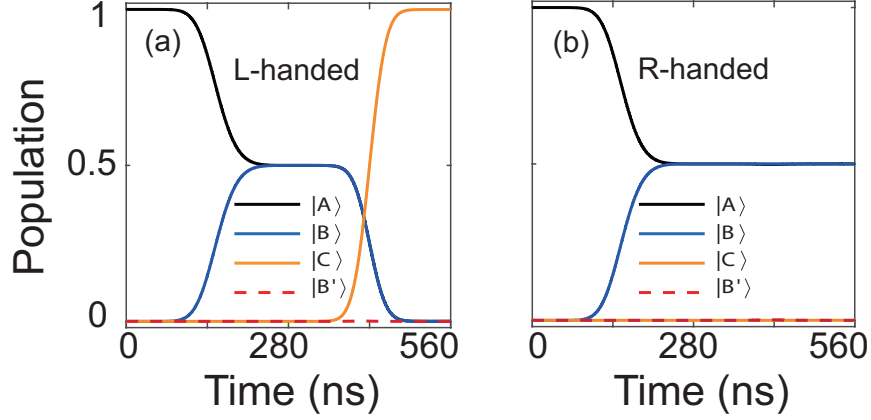


FIG. 3. The time-dependent populations of four rotational states for ESST to the state $|C\rangle$. The simulations for (a) the left-handed and (b) right-handed enantiomers with the duration $\tau_0 = 35\text{ns}$ and phase $\phi_a = \pi/2$.

For the target state $|C\rangle$, we set the parameters $A_a = \pi/(4\mu_a)$, $A_b = \pi/(2\sqrt{2}\mu_b)$, and $A_c = \pi/(2\sqrt{2}\mu_c)$. It is easy to verify that the three control fields defined by Eq. (22) with different values of τ_0 exactly satisfy the amplitude conditions in Eq. (14) at transition frequencies by fixing the center frequencies $\omega_a = \omega_{AB}$, $\omega_b = \omega_{AC}$ and $\omega_c = \omega_{BC}$. Figure 2 shows the results of $P_C^{L,R}(t_f)$ versus τ_0 and ϕ_a with $\phi_b = \phi_c = 0$. As expected, the ESST to the state $|C\rangle$ appears and depends highly on the phase values of ϕ_a . The fidelity of $P_C^{L,R}(t_f) > 0.999$ can be reached for $\tau_0 > 35$ ns, indicating that the unwanted transition to the neighboring state $|B'\rangle$ can be ignored. Figures 2 (b) and (e) plot the dependence of $P_C^{L,R}(t_f)$ on the phase ϕ_a for the case of $\tau_0 = 35$ ns. There is no ESST at $\phi_a = 0$ and π . The entire ESST to the left-handed molecule occurs at $\phi_a = \pi/2$ and a phase change to $\phi_a = 3\pi/2$ results in an opposite transfer to the right-handed one. The similar features can be observed by changing the values of ϕ_b (or ϕ_c) while choosing $\phi_a = \phi_c = 0$ (or $\phi_a = \phi_b = 0$). These results are in good agreement with the theoretical prediction by the phase conditions as well as previous M3WM experiments.

To visualize the underlying quantum state transfer mechanism, Fig.3 shows the time-dependent populations of the four states induced by the control fields for the cases of $\tau_0 = 35$ ns and $\phi_a = \pi/2$. For the two enantiomers, there are no visible populations in the state $|B'\rangle$ during the whole process. The four-level system is equivalent to the present closed-loop three-level model with the used pulse parameters. The control field $\mathcal{E}_a(t)$ with the pulse-areas $\theta_a(t_1) = \pi/4$ drives the system to the maximal coherent superposition of $|A\rangle$ and $|B\rangle$ with $P_A^{L,R}(t_1) = P_B^{L,R}(t_1) = 0.5$ for both enantiomers.

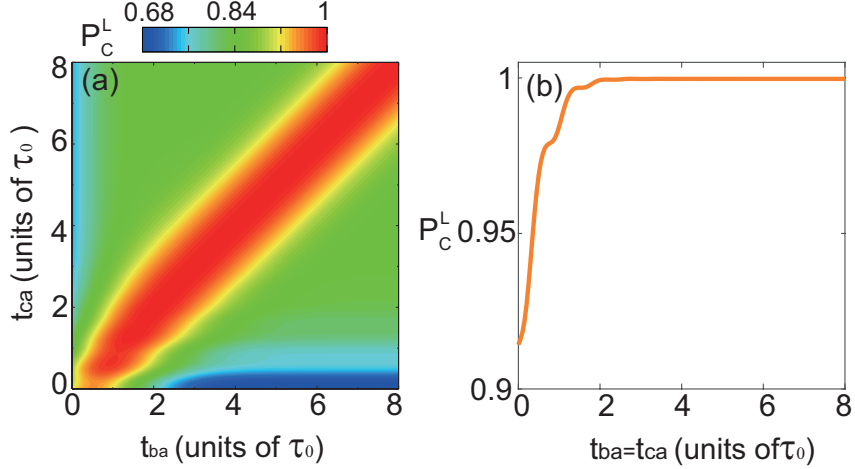


FIG. 4. The dependence of ESST on the time delays of control fields for the target state $|C\rangle$. (a) The final population of the left-handed enantiomer $P_C^L(t_f)$ versus the time delays $t_{ba} = t_b - t_a$ and $t_{ca} = t_c - t_a$. (b) The cut line plot of $P_C^L(t_f)$ along $t_{ba} = t_{ca}$.

Due to the sign difference of the transition from $|A\rangle$ to $|B\rangle$, $\mathcal{E}_a(t)$ with a phase $\phi_a = \pi/2$ will result in the phase of the state $|B\rangle$ in 0 and π for the left- and right-handedness, respectively, as described by Eq. (9). For the left-handedness, the transition path from $|A\rangle$ to $|C\rangle$ induced by $\mathcal{E}_b(t)$ will constructively with the path from $|B\rangle$ to $|C\rangle$ by $\mathcal{E}_c(t)$, leading to entire ESST to $|C\rangle$. For the right-handedness, however, the two paths are destructive, which keeps the molecules in the states $|A\rangle$ and $|C\rangle$, as shown in Fig. 3 (a) and (b).

As can be seen from our theoretical derivations, we divide the closed-loop excitation scheme into two time-separated stages. To see whether the amplitude and phase conditions can be applied to the overlapped cases, as an example, Fig. 4 plots the landscape of $P_C^L(t_f)$ with respect to the time delays $t_{ba} = t_b - t_a$ and $t_{ca} = t_c - t_a$ while fixing the center time t_a unchanged. $P_C^L(t_f)$ strongly depends on the overlap between two control fields of the second stage. Interestingly, $P_C^L(t_f)$ remains the value of $P_C^L(t_f) > 0.999$ for $t_{ba} = t_{ca} > 2\tau_0$ when $\mathcal{E}_b(t)$ and $\mathcal{E}_c(t)$ are turned on simultaneously with $t_{ba} = t_{ca}$. Even the three control fields are applied without any delays, high fidelity of $P_C^L(t_f) > 0.90$ holds, as shown in Fig. 4 (b). The phenomena can also be observed for the right-handedness (not shown here).

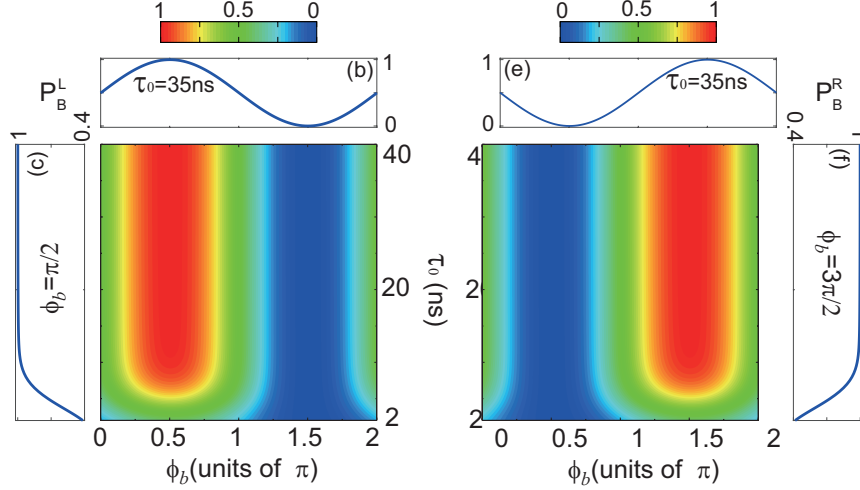


FIG. 5. Chiral dependence of ESST on the phase for the target state $|B\rangle$. (a) The final population of the left-handed enantiomer $P_C^L(t_f)$ versus the duration τ_0 and phase ϕ_b in a range of $[0, 2\pi]$, and the corresponding cut lines at (b) $\tau_0 = 35$ ns and (c) $\phi_b = \pi/2$. (d)-(f) The same plots as (a)-(c) for the right-handed enantiomer except for $\phi_a = 3\pi/2$ in (f).

B. ESST to $|B\rangle$

Figure 5 examines the same simulations as Fig. 2 but for the target $|B\rangle$ with $\phi_a = \phi_c = 0$. In our simulations, we choose the parameters $A_b = \pi/(4\mu_a)$, $A_a = \pi/(2\sqrt{2}\mu_b)$, and $A_c = \pi/(2\sqrt{2}\mu_c)$ so as to the all fields satisfy the amplitude conditions. The influence of the state $|B'\rangle$ looks more visible than that in Fig. 2 in the short duration regime, which becomes rather weak by increasing duration τ_0 . The final population $P_B^{L,R}(t_f)$ can also reach high fidelity for $\tau_0 > 35$ ns. As demonstrated in Fig. 2, the landscape of $P_B^{L,R}(t_f)$ exhibits a chiral symmetry with respect to the phase ϕ_b , for which the control field $\mathcal{E}_b(t)$ with $\phi_b = \pi/2$ leads to entire ESST to $|B\rangle$ of the left-handedness. For the right-handedness, however, it requires to $\phi_b = 3\pi/2$. This dependence of $P_B^{L,R}(t_f)$ on the phase is consistent with the theoretical predication.

Figure 6 plots the time-dependent populations of the system with $\tau_0 = 35$ and $\phi_b = \pi/2$. Since the transition moments μ_b are identical for the two enantiomers without a difference of sign, $\mathcal{E}_b(t)$ plays the same role in the first stage, generating the same maximal coherent superposition of $|A\rangle$ and $|C\rangle$. The constructive or destructive interference that depends on μ_a occurs between the transition paths from $|A\rangle$ and $|C\rangle$ to $|B\rangle$. As a result, the left-handed enantiomer is fully transferred to the state $|B\rangle$, whereas the right-handed one is still in the coherent states $|A\rangle$ and $|B\rangle$ at end of

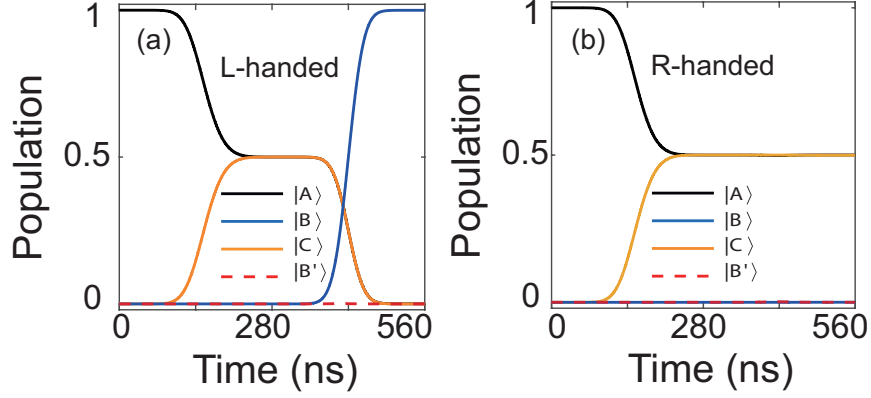


FIG. 6. The time-dependent populations of four rotational states for ESST to the state $|B\rangle$. The simulations for (a) the left-handed and (b) right-handed enantiomers with the duration $\tau_0 = 35\text{ns}$ and phase $\phi_b = \pi/2$.

three pulses.

To see the robustness of the scheme on the time delays, Fig. 7 examines the dependence

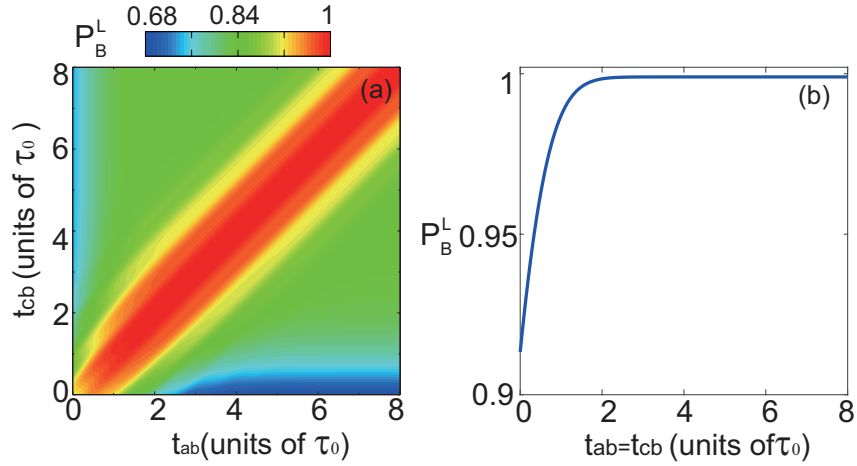


FIG. 7. The dependence of ESST on the time delays of control fields for the target state $|B\rangle$. (a) The final population of the left-handed enantiomer $P_B^L(t_f)$ versus the time delays $t_{ba} = t_b - t_a$ and $t_{ca} = t_c - t_a$. (b) The cut line plot of $P_B^L(t_f)$ along $t_{ba} = t_{ca}$.

of $P_B^L(t_f)$ on the time delays $t_{ab} = t_a - t_b$ and $t_{cb} = t_c - t_b$. Similar behaviors can be observed, indicating that both excitation schemes do not require strict separations between the control fields. The identical delays of the second stage fields are beneficial for the control. As a result, the amplitude and phase conditions can also be used for the overlapped control fields, leading to the high selectivity of handedness.

C. ESST with center frequency-detuned pulses

Finally, we examine the amplitude and phase conditions of control fields whose center frequencies $\omega_{a/b/c}$ are not exactly resonant with the transition center frequencies ω_{AB} , ω_{BC} and ω_{AC} . As can be seen from the definitions of the complex pulse areas $\theta_{a/b/c}(t_f)$, when the center frequencies are detuned away from resonances, the values of $|\theta_{a/b/c}(t_f)|$ will be decreased while keeping the parameters $A_{a/b/c}$ unchanged as used in resonant cases. We can increase the values of $A_{a/b/c}$ to revive the values of $\theta_{a/b/c}(t_f)$ at the transition frequencies so as to satisfy the amplitude conditions. That is, ESST in principle could be achieved by using the center-frequency-detuned pulses, as long as they satisfy the amplitude and phase conditions $\mathcal{E}_{a/b/c}$ and $\phi_{a/b/c}$ at transition frequencies.

Figure 8 shows the dependence of $P_B^L(t_f)$ on the detunings, for which the analytical simula-

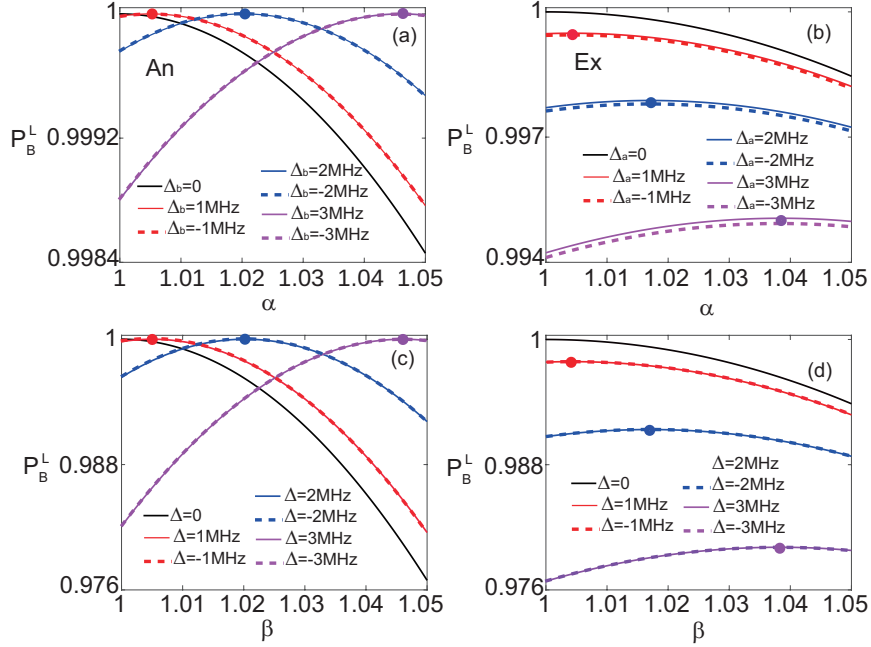


FIG. 8. The dependence of ESST on the detunings for the target state $|B\rangle$. and (b) The final population $P_B^L(t_f)$ versus the scale factor α of the coupling $\Omega_b(t)$ for different values of detuning $\Delta_b = \omega_b - \omega_{AC}$. (c) and (d) The final population $P_B^L(t_f)$ versus the scale factor β of the couplings $\Omega_a(t)$ and $\Omega_c(t)$ by taking $\Delta_a = \omega_a - \omega_{AB} = \Delta_c = \omega_c - \omega_{BC} = \Delta$. The analytical simulations (left panels) are compared with the exact results (right panels).

tions (left panels) are compared with the exact ones (right panels). We perform the simulations in Figs. 8 (a) and (b) to calculate $P_B^L(t_f)$ for different values of $\Delta_b = \omega_b - \omega_{AC}$ while scaling the coupling $\Omega_b(t)$ with a factor α , for which the center frequencies ω_b and ω_c are fixed at the reso-

nant conditions. The simulations in Figs. 8 (c) and (d) are accomplished with different detunings $\Delta_a = \omega_a - \omega_{AB}$ and $\Delta_c = \omega_c - \omega_{BC}$ by scaling the couplings $\Omega_a(t)$ and $\Omega_c(t)$ with a factor β , for which we set $\Delta_a = \Delta_c = \Delta$ while fixing $\Delta_b = 0$. For both analytical simulations, we can see that the detunings decrease $P_B^L(t_f)$. By increasing the strengths of the control fields, the maximal value of $P_B^L(t_f)$ can be revived to the same level as the resonant excitation, as shown in Figs. 8 (a) and (c). For the exact simulations, however, the maximal values can be increased but below the theoretical maximum. The differences can be attributed to the influence of high-order Magnus expansion terms, which are ignored in the analytical model. We also observe similar results for target state $|B\rangle$ (not shown here). Thus, the center-frequency detuned excitations with small detunings are also allowed by applying the corresponding amplitude and phase conditions at transition frequencies, whereas the larger detunings will reduce the ESST efficiency due to the optical processes via high-order high-order Magnus terms.

IV. CONCLUSION

We presented a general pulse-areas theorem analysis to explore ESST within a closed-loop three-level system. We considered three rotational states cyclically connected by the *a*-type, *b*-type, and *c*-type components of the transition dipole molecules. Using a strategy that separates the closed-loop excitation into two stages, we derived the amplitude and phase conditions for designing three linearly polarized microwave pulses to generate ESST to different targets. The two-stage strategy we used differs from previous schemes that turned on the direct one-photon transition from the initial state to the target state before the indirect two-photon one. Our schemes firstly switched on one control field involved in the two-photon path by generating maximal coherent supposition between the initial and intermediate states. We examined this three-level pulse-areas theorem in the cyclohexylmethanol molecules and analyzed its applications with both center-frequency resonant and detuned pulse sequences. For the latter, small detunings on the center frequencies of the control pulses would be expected to reduce the influence of high-order Magnus expansion terms. It opens a fundamental question of whether one can design fast and robust quantum control schemes against center-frequency detunings. To that end, optimal and robust control methods combined with artificial intelligence algorithms could be used to search for shaped control pulses subject to multiple constraints [51, 60–63].

ACKNOWLEDGMENTS

This work was supported by the National Natural Science Foundations of China (NSFC) under Grant No. 61973317. Y. G. is partially supported by the Scientific Research Fund of Hunan Provincial Education Department under Grant No. 20A025, Changsha Municipal Natural Science Foundation under Grant No. kq2007001, the Opening Project of Key Laboratory of Low Dimensional Quantum Structures and Quantum Control of the Ministry of Education under Grant No. QSQC1905, and the Open Research Fund of Hunan Provincial Key Laboratory of Flexible Electronic Materials Genome Engineering under Grant No. 202009.

- [1] L. Pasteur, Recherches sur les relations qui peuvent exister entre la forme cristalline, la composition chimique et le sens de la polarisation rotatoire, *Ann. Phys. Chem.* **24**, 442 (1848).
- [2] M. Quack, J. Stohner, and M. Willeke, High-resolution spectroscopic studies and theory of parity violation in chiral molecules, *Annu. Rev. Phys. Chem.* **59**,741 (2008).
- [3] R. Naaman and D. H. Waldeck, Spintronics and chirality: spin selectivity in electron transport through chiral molecules. *Annu. Rev. Phys. Chem.* **66**, 263 (2015).
- [4] R. Naaman, Y. Paltiel, and D. H. Waldeck, Chiral molecules and the electron spin. *Nat. Rev. Chem.* **3**, 250 (2019).
- [5] M. R. Wasielewski, M. D. E. Forbes, N. L. Frank, K. Kowalski, G. D. Scholes, J. Yuen-Zhou, M. A. Baldo, D. E. Freedman, R. H. Goldsmith, T. Goodson III, M. L. Kirk, J. K. McCusker, J. P. Ogilvie, D. A. Shultz, S. Stoll, and K. B. Whaley , Exploiting chemistry and molecular systems for quantum information science. *Nat. Rev. Chem.* **4**, 490 (2020).
- [6] C. Vogt, Separation of D/L-carnitine enantiomers by capillary electrophoresis, *J. Chromatogr. A* **745**,53 (1996).
- [7] R. M. Hazen and D. S. Sholl, Chiral selection on inorganic crystalline surfaces, *Nat. Mater.* **2**, 367 (2003).
- [8] D. Patterson and M. Schnell, New studies on molecular chirality in the gas phase: enantiomer differentiation and determination of enantiomeric excess. *Phys. Chem. Chem. Phys.* **16**, 11114 (2014).
- [9] G. Heppke, A. Jákli, S. Rauch, and H. Sawade, Electric-field-induced chiral separation in liquid crystals, *Phys. Rev. E* **60**,5575 (1999).

- [10] P. Brumer, E. Frishman, and M. Shapiro, Principles of electric-dipole-allowed optical control of molecular Chirality, *Phys. Rev. A* **65**, 015401 (2001).
- [11] I. Thanopoulos, P. Král, and M. Shapiro, Theory of a two-step enantiomeric purification of racemic mixtures by optical means: The $D_2 S_2$ molecule, *J. Chem. Phys.* **119**, 5105 (2003).
- [12] E. Frishman, M. Shapiro, and P. Brumer, Optical purification of racemic mixtures by laser distillation in the presence of a dissipative bath, *J. Phys. B: At. Mol. Opt. Phys.* **37**, 2811 (2004).
- [13] Y. Li, C. Bruder, and C. P. Sun, Generalized Stern-Gerlach effect for chiral molecules, *Phys. Rev. Lett.* **99**, 130403 (2007).
- [14] Y. Li and C. Bruder, Dynamic method to distinguish between left- and right-handed chiral molecules, *Phys. Rev. A* **77**, 015403 (2008).
- [15] C. Ye, Q. Zhang, and Y. Li, Real single-loop cyclic three-level configuration of chiral molecules, *Phys. Rev. A* **98**, 063401 (2018).
- [16] C. Ye, Q. Zhang, Y. Chen, and Y. Li, Effective two-level models for highly efficient inner-state enantioseparation based on cyclic three-level systems of chiral molecules, *Phys. Rev. A* **100**, 043403 (2019).
- [17] A. Yachmenev, J. Onvlee, E. Zak, A. Owens, and J. Küpper, Field-induced diastereomers for chiral separation, *Phys. Rev. Lett.* **123**, 243202 (2019).
- [18] J.-L. Wu, Y. Wang, J.-X. Han, C. Wang, S.-L. Su, Y. Xia, Y. Jiang, and J. Song, Two-path interference for enantiomer-selective state transfer of chiral molecules, *Phys. Rev. Applied* **13**, 044021 (2020).
- [19] B. T. Torosov, M. Drewsen, and N. V. Vitanov, Efficient and robust chiral resolution by composite pulses, *Phys. Rev. A* **101**, 063401 (2020).
- [20] B. T. Torosov, M. Drewsen, and N. V. Vitanov, Chiral resolution by composite Raman pulses, *Phys. Rev. Research* **2**, 043235 (2020).
- [21] C. Ye, Q. Zhang, Y. Chen, and Y. Li, Fast Enantioconversion of chiral mixtures based on a four-level double- Δ model, *Phys. Rev. Research* **2**, 033064 (2020).
- [22] J.-L. Wu, Y. Wang, S.-L. Su, Y. Xia, Y. Y. Jiang, and J. Song, Discrimination of enantiomers through quantum interference and quantum Zeno effect, *Opt. Express* **28**, 33475 (2020).
- [23] Y. Chen, C. Ye, Q. Zhang, and Y. Li, Enantio-discrimination via light deflection effect, *J. Chem. Phys.* **152**, 204305 (2020).
- [24] X. Xu, C. Ye, Y. Li, and A. Chen, Enantiomeric-excess determination based on nonreciprocal-transition-induced spectral-line elimination, *Phys. Rev. A* **102**, 033727 (2020).

- [25] C. Ye, B. Liu, Y.-Y. Chen, and Y. Li, Enantio-conversion of chiral mixtures via optical pumping, *Phys. Rev. A* **103**,022830 (2021).
- [26] I. Tutunnikov, L. Xu, R. W. Field, K. A. Nelson, Y. Prior, and I. S. Averbukh, Enantioselective orientation of chiral molecules induced by terahertz pulses with twisted polarization, *Phys. Rev. Research* **3**,013249 (2021).
- [27] K. Bergmann, H. Theuer, and B. W. Shore, Coherent population transfer among quantum states of atoms and molecules, *Rev. Mod. Phys.* **70**, 1003 (1998).
- [28] N. V. Vitanov, A. A. Rangelov, B. W. Shore, and K. Bergmann, Stimulated Raman adiabatic passage in physics, chemistry, and beyond, *Rev. Mod. Phys.* **89**, 015006 (2017).
- [29] X. Chen, I. Lizuain, A. Ruschhaupt, D. Guéry-Odelin, and J. G. Muga, Shortcut to adiabatic passage in two- and three-level atoms, *Phys. Rev. Lett.* **105**, 123003 (2010).
- [30] D. Guéry-Odelin, A. Ruschhaupt, A. Kiely, E. Torrontegui, S. Martínez-Garaot, and J. G. Muga, Shortcuts to adiabaticity: concepts, methods, and applications, *Rev. Mod. Phys.* **91**, 045001 (2019).
- [31] M. Shapiro, E. Frishman, and P. Brumer, Coherently controlled asymmetric synthesis with achiral light, *Phys. Rev. Lett.* **84**,1669 (2000).
- [32] P. Kra'1 and M. Shapiro, Cyclic population transfer in quantum systems with broken symmetry, *Phys. Rev. Lett.* **87**, 183002 (2001).
- [33] P. Kra'1, I. Thanopoulos, M. Shapiro, and D. Cohen, Two-step enantio-selective optical switch, *Phys. Rev. Lett.* **90**, 033001 (2003).
- [34] D. Gerbasi, M. Shapiro, and P. Brumer, Theory of enantiomeric control in dimethylallene using achiral light, *J. Chem. Phys.* **115**,5349 (2001).
- [35] N. V. Vitanov and M. Drewsen, Highly efficient detection and separation of chiral molecules through shortcuts to adiabaticity, *Phys. Rev. Lett.* **122**,173202 (2019).
- [36] J. Wu, Y. Wang, J. Song, Y. Xia, S. Su, and Y. Jiang, Robust and highly efficient discrimination of chiral molecules through three-mode parallel paths, *Phys. Rev. A* **100**,043413 (2019).
- [37] E. Frishman, M. Shapiro, D. Gerbasi, and P. Brumer, Enantiomeric purification of nonpolarized racemic mixtures using coherent light, *J. Chem. Phys.* **119**,7237 (2003).
- [38] H. R. Hamedí, E. Paspalakis, G. Žlabys, G. Juzeliūnas, and J. Ruseckas, Complete energy conversion between light beams carrying orbital angular momentum using coherent population trapping for a coherently driven double- Λ atom-light-coupling scheme, *Phys. Rev. A* **023811**; **102**, 019903(E) (2020).

- [39] D. Patterson and J. M. Doyle, Sensitive chiral analysis via microwave three-wave mixing, *Phys. Rev. Lett.* **111**,023008 (2013).
- [40] D. Patterson, M. Schnell, and J. M. Doyle, Enantiomer-specific detection of chiral molecules via microwave spectroscopy, *Nature* **497**, 475 (2013).
- [41] V. A. Shubert, D. Schmitz, D. Patterson, J. M. Doyle, and M. Schnell, Identifying enantiomers in mixtures of chiral molecules with broadband microwave spectroscopy, *Angew. Chem. Int. Ed.* **53**, 1152 (2014).
- [42] V. A. Shubert, D. Schmitz, C. Medcraft, A. Krin, D. Patterson, J. M. Doyle, and M. Schnell, Rotational spectroscopy and three-wave mixing of 4-Carvomenthenol: a technical guide to measuring chirality in the microwave regime, *J. Chem. Phys.* **142**, 214201 (2015).
- [43] S. Lobsiger, C. Pérez, L. Evangelisti, K. K. Lehmann, and B. H. Pate, Molecular structure and chirality detection by fourier transform microwave spectroscopy, *J. Phys. Chem. Lett.* **6**, 196 (2015).
- [44] S. Eibenberger, J. Doyle, and D. Patterson, Enantiomer-specific state transfer of chiral molecules, *Phys. Rev. Lett.* **118**, 123002 (2017).
- [45] S. R. Domingos, C. Perez, and M. Schnell, Sensing chirality with rotational spectroscopy, *Annu. Rev. Phys. Chem.* **69**, 499 (2018).
- [46] C. Pérez, A. L. Steber, A. Krin, and M. Schnell, Statespecific enrichment of chiral conformers with microwave spectroscopy, *J. Phys. Chem. Lett.* **9**, 4539 (2018).
- [47] M. Leibscher, T. F. Giesen, and C. P. Koch, Principles of enantio-selective excitation in three-wave mixing spectroscopy of chiral molecules, *J. Chem. Phys.* **151**,014302 (2019).
- [48] D. Sugny and C. Kontz, Optimal control of a three-level quantum system by laser fields plus von Neumann measurements, *Phys. Rev. A* **77**,063420 (2008).
- [49] Y. Guo, L. Zhou, L. M. Kuang, and C. P. Sun, Magneto-optical Stern-Gerlach effect in an atomic ensemble. *Phys. Rev. A* **78**, 013833 (2008).
- [50] G. Shchedrin, C. O'Brien, Y. Rostovtsev, and M. O. Scully, Analytic solution and pulse area theorem for three-level atoms, *Phys. Rev. A* **92**,063815 (2015).
- [51] Y. Guo, X. B. Luo, S. Ma, and C.-C. Shu, All-optical generation of quantum entangled state with strict constrained ultrafast laser pulses, *Phys. Rev. A* **100**, 023409 (2019).
- [52] B. Y. Chang, I. R. Sola, and V. S. Malinovsky, Anomalous rabi oscillations in multilevel quantum systems, *Phys. Rev. Lett.* **120**,133201 (2018).

- [53] H. Mineo, G.-S. Kim, S. H. Lin, and Y. Fujimura, Dynamic stark-induced coherent π -electron rotations in a chiral aromatic ring molecule: application to phenylalanine, *J. Phys. Chem. A*. **123**,6399 (2019).
- [54] Y Guo, C.-C. Shu, D. Y. Dong, and F. Nori, Vanishing and revival of resonance Raman scattering, *Phys. Rev. Lett.* **123**,223202 (2019).
- [55] C.-C. Shu, Q.-Q. Hong, Y. Guo, and N. E. Henriksen, Orientational quantum revivals induced by a single-cycle terahertz pulse, *Phys. Rev. A* **102**, 063124 (2020).
- [56] C.-C. Shu, Y. Guo, K.-J. Yuan, D. Y. Dong, and A. D. Bandrauk, Attosecond all-optical control and visualization of quantum interference between degenerate magnetic states by circularly polarized pulses. *Opt. Lett.* **45**, 960 (2020).
- [57] Q.-Q. Hong, L.-B. Fan, C.-C. Shu and N. E. Henriksen, Generation of maximal three-state field-free molecular orientation with terahertz pulses, *Phys. Rev. A* **104**, 013108 (2021).
- [58] S. Blanes, F. Casas, J. A. Oteo, and J. Ros, The Magnus expansion and some of its applications, *Phys. Rep.* **470**, 151 (2009).
- [59] K. K. Lehmann, Influence of spatial degeneracy on rotational spectroscopy: three-wave mixing and enantiomeric state separation of chiral molecules, *J. Chem. Phys.* **149**, 094201 (2018).
- [60] C.-C. Shu, T.-S. Ho, X. Xing, and H. Rabitz, Frequency domain quantum optimal control under multiple constraints. *Phys. Rev. A* **93**, 033417 (2016).
- [61] Y. Guo, D. Dong, and C.-C. Shu, Optimal and robust control of quantum state transfer by shaping spectral phase of ultrafast laser pulses. *Phys. Chem. Chem. Phys.* **20**, 9498 (2018).
- [62] D. Dong, C.-C. Shu, J. C. Chen, X. Xing, H. L. Ma, Y. Guo, and H. Rabitz, Learning control of quantum systems using frequency-domain optimization algorithms. *IEEE Trans. Control. Syst Technol.* **29**, 1791 (2021).
- [63] X. W. Liu, G. J. Zhang, J. Li, G. L. Shi, M. Y. Zhou, B. Q. Huang, Y. J. Tang, X.H. Song, and W.F. Yang, Deep learning for Feynman's path integral in strong-field time-dependent dynamics, *Phys. Rev. Lett.* **124**, 113202 (2020).